NUCL SCI TECH (2018) 29:142
https://doi.org/10.1007/s41365-018-0478-x

RF tuning and beam commissioning of CW RFQ for China-ADS Injector-I

Hua Shi[1] · Huafu Ouyang[1] · Shengchang Wang[1] · Ningchuang Zhou[1] · Gang Wu[1]

Received: 8 February 2018 / Revised: 8 April 2018 / Accepted: 7 May 2018 / Published online: 29 August 2018

Abstract A 325-MHz continuous-wave (CW) four-vane radiofrequency quadrupole (RFQ) is employed in Injector-I of the China Accelerator-Driven Subcritical System. The radiofrequency tuning and beam commissioning were performed from January 2014 to January 2017. In a cold test, a stability study showed that the design of the segmented resonantly coupling and dipole stabilizer rods can shift the harmful quadrupole and dipole mode from the fundamental mode to above 2.6 MHz. We also found a simplified tuning method for the field unflatness, involving changing the inserted length of a few plug tuners. For achieving CW-beam commissioning, two full-size RFQs were constructed successively. The commissioning results indicate that the beam transmission rate decreased by approximately 3% as the normalized field unflatness decreased by 1%. A 10-MeV CW proton beam with an average beam current of 2.1 mA was achieved at the target of Injector-I, and the output beam energy of the RFQ was 3.18 MeV.

Keywords RFQ · RF tuning · CW-beam commissioning · beam transmission rate

✉ Hua Shi
shih@ihep.ac.cn

[1] Key Laboratory of Particle Acceleration Physics and Technology, Institute of High Energy Physics, Chinese Academy of Sciences, Beijing 100049, China

1 Introduction

The China Accelerator-Driven Subcritical System (China-ADS) Injector-I is designed to operate in the continuous-wave (CW) mode at 325 MHz. It employs an electron cyclotron resonance (ECR) ion source, a low-energy transport line, a radiofrequency quadrupole (RFQ) accelerator, and a superconducting section with energy of 10 MeV and a beam current of 10 mA [1]. A four-vane RFQ accelerator has been developed to accelerate proton beams from 35 keV to 3.2 MeV.

In a dynamic study, two-dimensional (2D) and three-dimensional (3D) radiofrequency (RF) design and thermal analysis were performed. The main design parameters are summarized in Table 1 [2]. The output beam current is 15 mA, which is higher than the operation value of 10 mA for a possible upgrade. The RF power dissipation with an inter-vane voltage of 55 kV is approximately 194.96 kW, and the maximum surface field is 28.88 MV/m, as given by Superfish [3]. Considering the contribution of the 3D structure, the actual cavity power dissipation is generally 1.2–1.4 times the Superfish 2D value. The beam transmission rate is proposed to be $> 98.7\%$ for reducing the CW-beam power loss. The output normalized root-mean-square (rms) emittances ($x/y/z$) are 0.2/0.2/0.0612 (πmm mrad/πmm mrad/MeV deg), and a small growth of emittances is required. The 4.7-m-long RFQ is composed of four modules each < 1.2 m long, which are easily fabricated, as well as a water-cooling system.

It is very important to restrict the beam loss and reduce the emittance growth for the CW-mode high-intensity RFQ; thus, the RFQ requires good field unflatness of $\frac{\Delta E}{E} \leq \pm 2.5\%$ [4–6] and high stability [7–10]. To achieve these requirements, the machining and alignment errors

Table 1 Main RFQ design parameters [2]

Parameters	Value
Frequency (MHz)	325
Particle	H^+
Injection energy (keV)	35
Output energy (MeV)	$\sim$ 3.2
Output beam current (mA)	15 (10 operation)
Beam duty factor	100%
Inter-vane voltage (kV)	55
Maximum surf. field (MV/m) (Superfish)	28.88 (Kilpatrick factor = 1.62)
Cavity power dissipation (kW) (Superfish)	194.96
Beam transmission rate	98.7%
Output norm. rms emittance ($x/y/z$) (πmm mrad/πmm mrad/MeV deg)	0.2/0.2/0.0612
Accelerator length (cm)	469.95

should be controlled within $\pm$ 15 and $\pm$ 10 μm, respectively, and several other stability designs and methods must be adopted. In addition to the coordinate machine measurement, alignment survey, cooling-water flow, and vacuum checking, RF measurement is a necessary procedure throughout the fabrication, installation, and commissioning. After a process is finished, a bead-pull measurement is taken, and the plug tuners are adjusted according to the testing results of RF measurement; then, the expected field unflatness can be achieved after several tuning procedures. Additionally, RF measurement is a valid method for assessing the deviation before and after a process, and the proper processing technology can be chosen with the help of RF measurement.

CW-mode high-power conditioning is also very important for a high-intensity RFQ [11, 12]. Two full-size RFQs based on the same physical design were fabricated for CW-beam commissioning. The inner surface of the first RFQ (RFQ-1) was severely damaged in high-power conditioning owing to the lack of conditioning experience; thus, CW-beam operation cannot be achieved. However, for the second RFQ (RFQ-2), 3.18-MeV CW proton beams have been achieved with the proper conditioning parameters and procedures.

The RF tuning of the RFQ is introduced. It includes four parts: (1) the RFQ structure; (2) the test facility; (3) a stability study, in which the method of increasing the mode frequency separation between harmful modes (dipole, quadrupole modes) and the operation quadrupole mode is determined, and the simulation and testing results of the final mode frequency separation values are presented; (4) a field unflatness tuning study, in which the method of improving the field unflatness is discussed in detail. A detailed high-power RF conditioning scheme is given in Sect. 3, and the problems in the RF conditioning and corresponding methods for improvement are presented. The beam-commissioning results of two RFQs are presented in Sect. 4, and the quantified relationship between the beam transmission rate and the field unflatness is discussed.

2 RF tuning

2.1 RFQ structure

A side view of the RFQ is shown in Fig. 1. Two segments are joined with a resonant coupling gap, and each segment includes two modules that are connected by flanges. The beam direction is from module 1 to module 4. Four couplers are installed in modules 2 and 3, and 16 vacuum ports lie inside modules 1 and 4. In the four modules, 64 plug tuners with a diameter of 55 mm are uniformly distributed. Two testing cables are usually connected to the tuners of adjacent upper quadrants with two RF pickups in the middle of a single module or the whole RFQ.

2.2 Test facility

As shown in Fig. 2, the test facility is composed of a single module (or whole RFQ), a vector network analyzer (VNA, Agilent E8720ES), a control computer, a bead-pull apparatus, a servomotor, etc. [13]. The computer communicates with the VNA through a general-purpose interface bus. The dielectric bead is pulled by a nylon wire via the servomotor across the vane gap near the top of the four quadrants one by one, where a strong electric field is located, as shown in Fig. 3. The four symmetric wire positioning slots are cut in the two end plates in order to ensure the accurate position. The bead-pull measurement setup with a single RFQ module is shown in Fig. 4, and the module is fixed in the marble platform.

The main measurement parameters are the frequency spectrum, electric-field phase, and Q-value, for both a

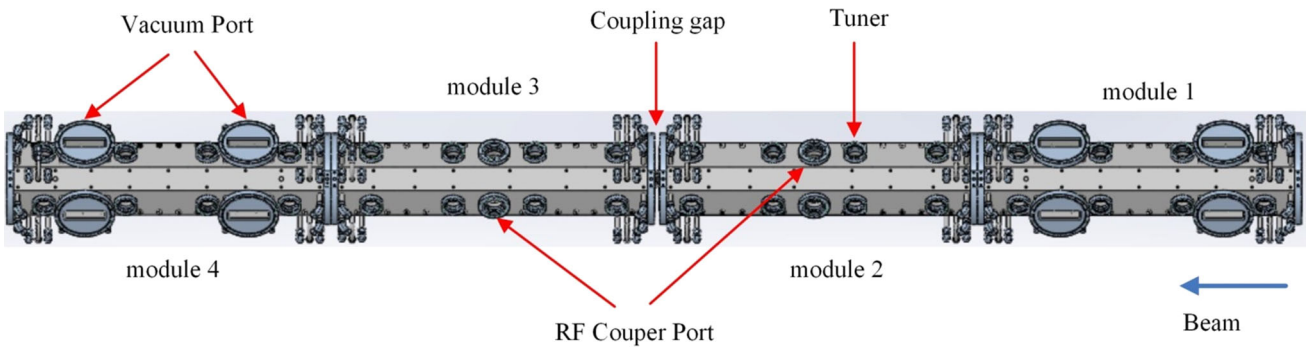

Fig. 1 RFQ side view

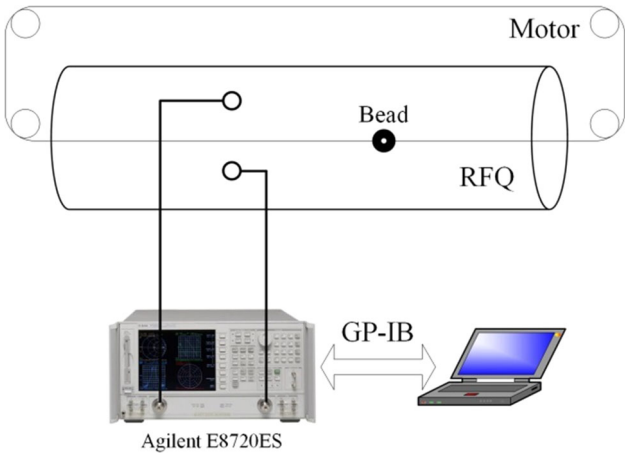

Fig. 2 RFQ test facility

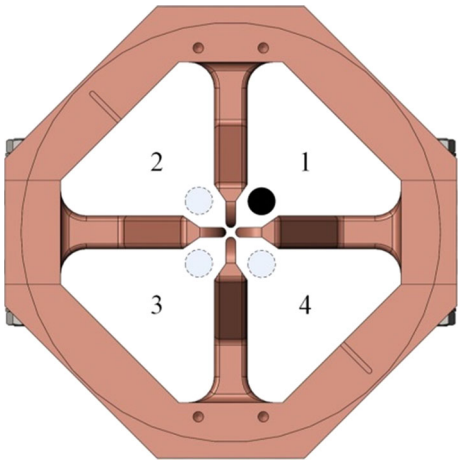

Fig. 3 Position of the bead

single module and the whole RFQ. Two programs are written, as follows.

1. Spectrum measurement program. This can give not only the spectrum of the fundamental quadrupole mode and neighboring harmful modes but also the frequency of modes after the measurement bandwidth is reduced.

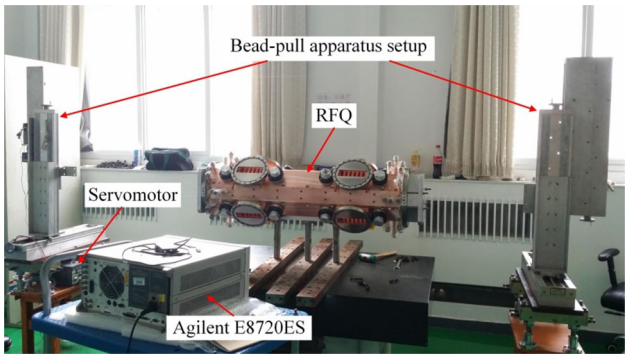

Fig. 4 Bead-pull apparatus setup

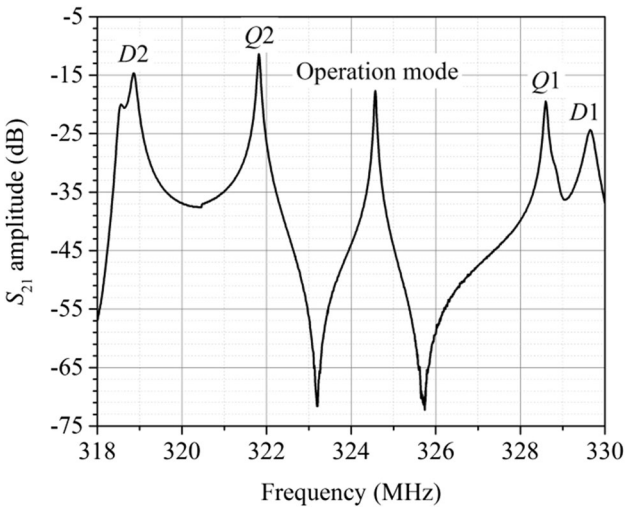

Fig. 5 Frequency spectrum of the RFQ

Figure 5 shows the frequency spectrum of the RFQ, two quadrupole modes $Q1$ and $Q2$, and two dipole modes $D1$ and $D2$.

2. Phase acquisition program. The S_{21} phase distribution curve for the fundamental mode is acquired, while the bead is pulled along the RFQ. When the cavity is in resonance, the field deviation caused by the bead is proportional to the square root of the perturbed

frequency deviation, i.e., the S_{21} phase deviation. Thus, we measure the perturbed S_{21} phase distribution instead of the field distribution. Before the measurement, the sweeping time when the bead is moving from one end plate to another should be tested. When all the fixed copper tuners are installed and the field unflatness satisfies the requirement, the phase deviation is $< 1°$, except for a 2° step at the coupling plate, as shown in Fig. 6. As shown later, with this phase deviation, the field distribution unflatness is better than $\pm$ 2.5%.

2.3 Stability study

Because the length of the RFQ is approximately five times the wavelength of the operation mode, the mode frequency separation between the harmful modes and the fundamental quadrupole mode is so small that the structural asymmetry resulting from errors in fabrication and installation can easily cause mode coupling. Thus, stabilization techniques should be employed to improve the longitudinal and transverse beam instability caused by mode coupling [7–10]. In China-ADS Injector-I, we adopted the following techniques. (1) Segment resonant coupling design. Two approximately 2.35-m-long RFQ segments are resonantly coupled together, and a small gap between the vane tips provides capacitive coupling. The frequency of the nearest quadrupole modes can be moved farther away from the operation mode by tuning the width of the gap. Figure 7 shows the final optimized size of the coupling cell, where the gap width is 1.4 mm, the thickness of the coupling plate is 18.2 mm, and the distance between the two vane undercuts is 79.8 mm. (2) Dipole stabilizer rod design. Four rods are located in each end plate of two segments. The frequency of the nearest dipole modes can be moved farther away from the operation mode by tuning the length of the rods. Figure 8 shows the coupling plate with dipole rods. The optimized length of the rods is 169 mm, according to simulation and cold-test results.

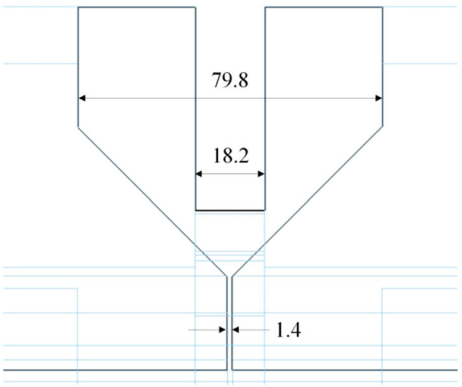

Fig. 7 Size of the coupling cell (unit: mm)

According to results obtained using 3D Computer Simulation Technology [14], the mode frequency separation values from the nearest quadrupole and dipole mode to the operation mode are approximately 1.5 and 0.2 MHz, respectively, without the resonant coupling of segments and the dipole stabilizer rod design. Considering the two techniques, according to the simulation results shown in Table 2, the mode frequency separation values increase to approximately 3.4 MHz (quadrupole modes) and 5.4 MHz (dipole modes) [2], respectively, where f_n is the frequency of each mode, and f_0 is that of the operation mode. Because of the inevitable fabrication and assembly errors, the testing results are all lower than the simulation results for RFQ-1 and RFQ-2. However, all the testing-mode frequency separation values are > 2.6 MHz, which is acceptable.

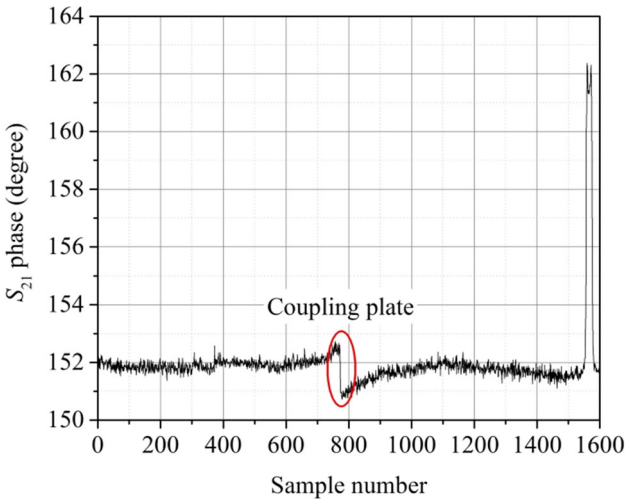

Fig. 6 Phase distribution with fixed copper tuners and the required field unflatness

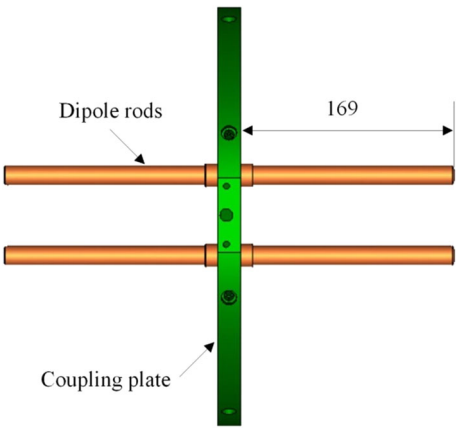

Fig. 8 Coupling plate with dipole rods (unit: mm)

Table 2 Comparison of mode frequency and separation values between simulation and measurement results

Modes	Simulation results [2]		Measurement results (RFQ-1)		Measurement results (RFQ-2)	
	Frequency (MHz)	f_n–f_0 (MHz)	Frequency (MHz)	f_n–f_0 (MHz)	Frequency (MHz)	f_n–f_0 (MHz)
*D*2	319.638	− 5.400	318.860	− 5.936	318.983	− 6.050
*Q*2	321.451	− 3.587	322.160	− 2.636	321.048	− 3.985
Fundamental mode	325.038	0	324.796	0	325.033	0
*Q*1	328.454	+ 3.416	328.660	3.864	327.926	2.893
*D*1	330.588	+ 5.550	329.670	4.874	329.912	4.879

2.4 Field unflatness tuning study

Although the tolerance is strictly controlled, there are errors in each fabrication procedure. Thus, numerous slug tuners are designed to tune and compensate the local field in order to achieve the required field unflatness. The local-field tuning program is written using perturbation and lumped-circuit theory [4–6]. This program can give the field distribution of the current test and calculate the adjustment of each slug tuner. The field unflatness can be gradually achieved after several adjustments.

Figure 9 shows the final normalized electric field of RFQ-1, where Quad-1–Quad-4 represent Quadrants 1–4, and $\frac{\Delta E}{E}$ is − 2.50% to + 2.44%. Figure 10 shows the normalized electric field of RFQ-2 with fixed copper tuners, and $\frac{\Delta E}{E}$ is − 2.65% to + 2.05%. Both of these configurations satisfy the design requirement.

However, there were two coaxial couplers with the wrong coupling-factor values in RFQ-2, and the value in Quadrant 4 coupler of module 3, which is opposite Quadrant 2, had a large deviation. The normalized electric field worsened to − 5.62% to + 8.09% after the tuning of the coupling factor. A magnetic-coupling coupler is adopted for the RFQ, and a different coupling factor means a

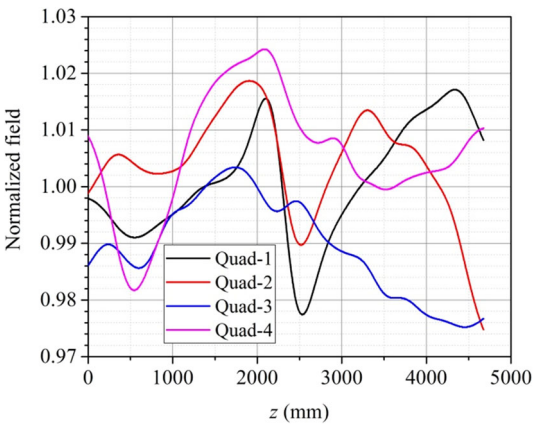

Fig. 9 Final normalized electric-field distribution of RFQ-1

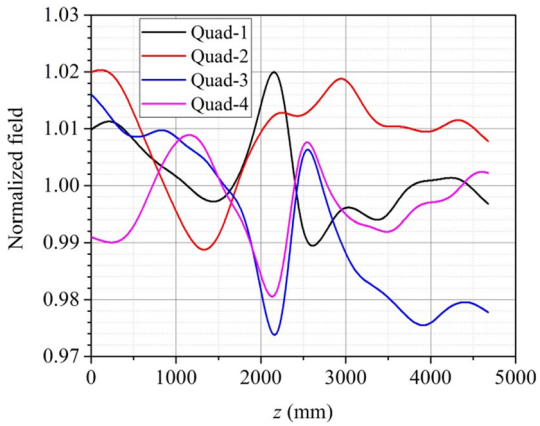

Fig. 10 Normalized electric-field distribution of RFQ-2 with fixed copper tuners

different local inductance and therefore a different local frequency. The local-frequency deviation in Quadrant 4 affects not only the field distribution in Quadrant 4 but also the field distribution in opposite Quadrant 2 for the intensive coupling between Quadrants 4 and 2. Physically, the local-frequency deviation caused by the coupler can be restored by the tuners near the coupler. As shown in Fig. 11a, the main field distortion arises from the significantly higher field value in Quadrant 2, and consequently, the fundamental frequency increases from 325.013 to 325.044 MHz, which agrees with the relationship between the local frequency and the local electric field in a cell for a coupling cavity with many cells [15]. Because all fixed copper tuners were machined and it is impossible to refabricate all the copper tuners and retune the field within the constraints of the project schedule and budget, it is necessary to improve the field unflatness by only replacing several fixed tuners.

According to the simulation results [2], the relationship between the local-frequency adjustment and the insertion length of one tuner is approximately 3.93 kHz/mm, and the two tuners in Quadrant 2 of module 3 should be the main influencing factors. When the two tuners are both pulled out by approximately 4 mm, the resonant frequency should

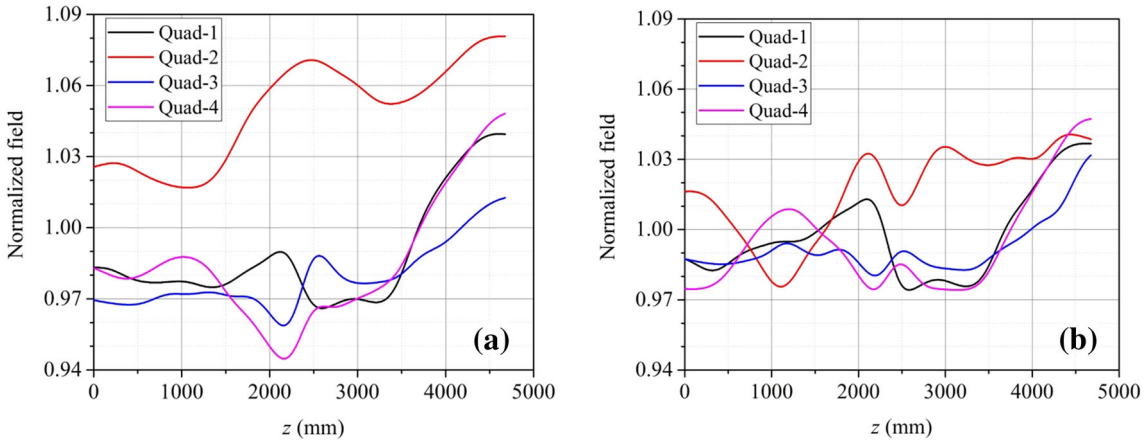

Fig. 11 Normalized electric-field distribution of RFQ-2: **a** before and **b** after tuning two tuners

recover. The fixed turners were replaced with two tunable aluminum tuners, and the lengths that the tuners were pulled out were identified to be 4.53 and 3.66 mm by tuning and testing the field and frequency locally. Figure 11b shows the final normalized electric field. The field unflatness and resonant frequency returned to − 2.63% to + 4.75% and 325.018 MHz, respectively. The beam transmission rate was predicted to decrease to 92–93%; however, this is acceptable.

3 High-power RF conditioning

The RF power of CW conditioning depends on the simulation and cold-test results. A high-frequency structure simulator [16] is used to achieve the following values: a quality factor of $Q_0 = 9163$, power dissipation of $P = 205.6$ kW, and a relationship of $Q_0 \propto 1/P$ between them. In the cold test, for example, the Q_0 of RFQ-2 decreased to 7833; accordingly, P increased to approximately 240 kW. The RF power was set as 270–280 kW in low-duty factor (< 30%) conditioning and 250–260 kW in high-duty factor or CW conditioning, and the additional power dissipation caused by the difference between the measurement and theory was considered.

The RF conditioning of RFQ-1 started on May 15, 2014, but several accidents or problems stopped the RF conditioning and resulted in a decrease in the RFQ performance [17]. On June 12, 2014, vacuum leakage occurred at the welding port in the entrance plate at a 71% RF duty factor and 250-kW power owing to the lack of cooling water, which resulted in a large temperature difference between the plate and rods. Figure 12a shows the damaged entrance plate. On June 20, 2014, vacuum leakage occurred at the welding port in the coupling plate at an 80% RF duty factor and 257-kW power, possibly because of a welding problem due to the complicated structure of the cooling-water channels. On July 20, 2014, an arc accompanied by a very low vacuum pressure was detected at coupler #4 [18]. After disassembling the coupler, a burned RF contact spring was found, as shown in Fig. 12b. The loose contact of the spring was thought to be the main reason; in this case, the fingers of the spring easily caused discharge under high-power conditioning. In April 2015, RFQ-1 could not be easily operated at a high RF duty factor, and vacuum interlock occurred frequently at or below the required RF power. Inner-surface damage of a large area was observed using an endoscope, as shown in Fig. 12c. This is mainly attributed to the lack of reflected power interlock protection, because the vacuum interlock with a millisecond reaction time was too slow to stop the discharge extending between the adjacent vanes. Another possible reason is that the purity of the copper was insufficient.

Considering the failures of RFQ-1, the new RFQ-2 was fabricated with higher-purity copper and several improvements, as follows. (1) It had simplified cooling-water channels in the end plates and coupling plate, as shown in Fig. 13a. Thermal analysis was performed using ANSYS [19], as shown in Fig. 13b, and the maximum temperature in the rod was < 29 °C at a water velocity of 2 m/s. The newly designed plates were tested in RFQ-1 [17]. (2) The RF contact spring was canceled in the new couplers [18], and a copper vacuum flange gasket was used for the RF contact. (3) New reflected power interlock protection was applied, and the protection strategy varied according to the RF pulse width and pulse duty factor.

The RF conditioning of RFQ-2 started on October 18, 2016, and the procedure from the pulse mode to the CW mode is shown in Fig. 14. It began with a very low-duty factor of 0.4% and high RF power of 280 kW. Then, the duty factor was extended to 40% with the same RF power by increasing the pulse width or repetition rate. From the 40% duty factor to the CW mode, the RF power and repetition rate were kept at 250–260 kW and 50 Hz,

Fig. 12 Damage in RFQ-1 commissioning: **a** entrance plate with damaged rods, **b** coupler #4 with a burned RF contact spring, and **c** inner-surface damage status of RFQ-1

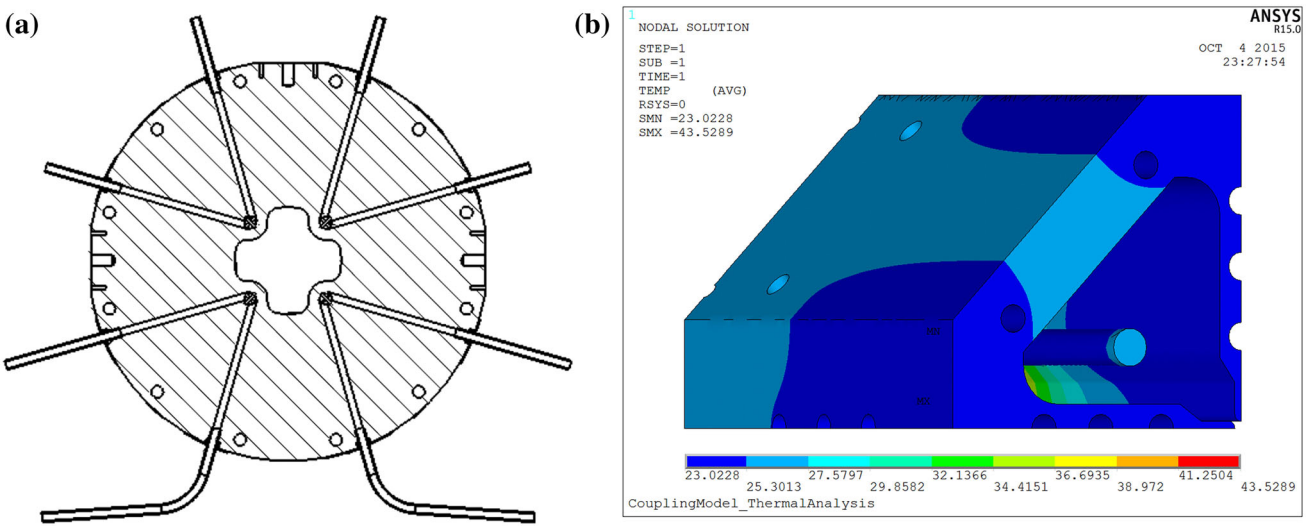

Fig. 13 **a** Cooling-water channel design and **b** thermal analysis of the end plates and coupling plate

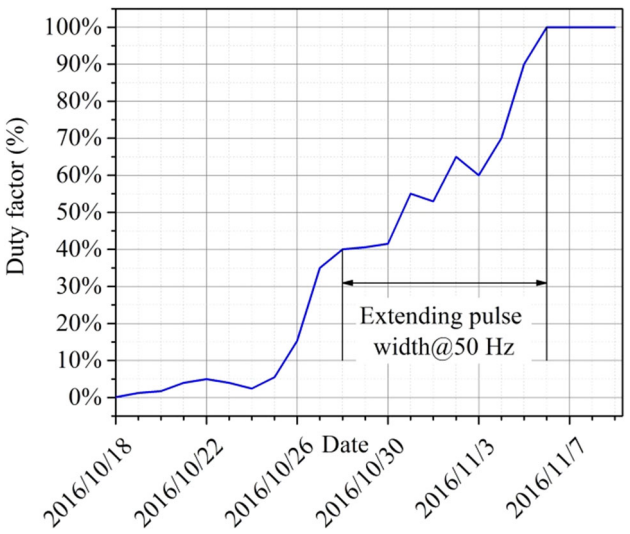

Fig. 14 RFQ-2 conditioning procedure

respectively, and the pulse width was increased from 8 to 20 ms because it is easy to transit from a long pulse to the CW mode. On November 17, 2016, the maximum RF power in the CW mode reached approximately 275 kW, but the electron flow near the ceramic window of one RF coupler was high; thus, the RF power decreased over the remaining 15 min. In the CW mode, RFQ-2 operated steadily for > 13 h at a 250–260-kW RF power.

4 Beam commissioning

The beam commissioning of RFQ-1 started on August 7, 2014, and the beam transmission rate reached approximately 97% below a 1% duty factor [20]. The beam commissioning above a 50% beam duty factor of RFQ-1 in 2014 is detailed in Table 3 [21]. The output peak current was > 10 mA for each duty factor, and the maximum RF power reached 314 kW. The beam transmission rate was 95% at a 70% beam duty factor and 90% at a 90% beam duty factor. The maximum average beam power was approximately 31 kW.

The beam commissioning of RFQ-2 started on December 4, 2016, and the transmission rate below a 1% duty

Table 3 Beam commissioning of RFQ-1 [21]

Beam duty factor	50%	60%	65%	70%	90%
Transmission rate	95%	95%	95.6%	95%	90%
RFQ output peak current (mA)	11.1	10.9	10.9	10.6	11
RFQ pulse width/repetition frequency (ms/Hz)	11/50	13/50	14/50	15/50	19/50
Power in the cavity (kW)	289	305	314	298	300
Experiment date	2014/9/1	2014/9/1	2014/9/1	2014/9/2	2014/9/25

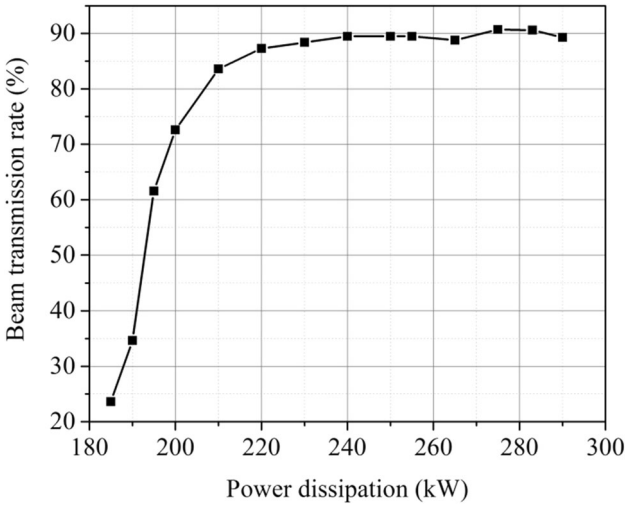

Fig. 15 Beam transmission rate in the pulse-beam mode of RFQ-2

factor is shown in Fig. 15. The maximum transmission rate was 90.7% at a 275-kW RF power, which is lower than the predicted value of approximately 92%. The main reason for this discrepancy is likely that the beam from the ECR proton ion source was not at the center of the aperture. In early 2017, China-ADS Injector-I achieved a CW beam with beam energy of 10 MeV and an average beam current of 2.1 mA, and the output energy of RFQ-2 was 3.18 MeV. RFQ-2 was considered to be able to deliver a beam current of up to 10 mA, but the SC section could not handle a high beam current [22].

On the basis of the beam-commissioning results of the two RFQs, with a very low RF duty factor and beam duty factor (almost no cavity deformation), at the same input RF power, the relationship between the beam transmission rate and the nominal field unflatness was 97%@− 2.50% to + 2.44% for RFQ-1 and 90.7%@− 2.63% to + 4.75% for RFQ-2. In this case, the difference in the beam transmission rate mainly arises from the field distribution unflatness. Thus, we estimate that the beam transmission rate decreased by approximately 3% with the field unflatness decreasing by 1%. Certainly, the exact relationship between the beam transmission rate and the field distribution unflatness can be determined via simulations.

5 Conclusion

A bead-pull apparatus setup was constructed, and testing programs were written. The stability was studied, and segments with resonant coupling and dipole stabilizer rods were adopted. The testing results for the mode frequency separation values between the harmful neighboring modes and the fundamental quadrupole mode were all > 2.6 MHz, which is sufficient for preventing mode coupling. A simplified tuning method for the field unflatness based on the perturbation theory and simulation results was developed. The normalized electric field of RFQ-2 was improved from − 5.62% to + 8.09% to − 2.63% to + 4.75% using this method.

The relationship between the field unflatness and the beam transmission rate was estimated according to the beam-commissioning results of the two RFQs. A 1% decrease in the normalized field unflatness corresponded to a decrease of approximately 3% in the beam transmission rate.

The beam commissioning of the 325-MHz four-vane RFQ in China-ADS Injector-I was successfully performed in both the pulse and CW modes. For RFQ-1, the maximum average beam power was 31 kW with a 95% RF pulse and a 90% beam-pulse duty factor, and the beam transmission rate was 90%. For RFQ-2, the output energy in the CW mode was 3.18 MeV at an approximately 260-kW RF power.

Acknowledgements The authors acknowledge the beam-commissioning group of China-ADS Injector-I for the cooperation and help in the beam commissioning.

References

1. J.Y. Tang, Z.H. Li et al., Conceptual physics design on the C-ADS accelerators. IHEP-CADS-Report/2012-01E (2012)
2. H.F. Ouyang, S.L. Pei, Physics design on C-ADS injector-1 RFQ. Prog. Rep. China Nucl. Sci. Technol. **2**, 66–73 (2011)
3. Superfish. http://laacg.lanl.gov/laacg/services/download_sf.phtml
4. S.N. Fu, Software development for the RF measurement and analysis of RFQ accelerator. HEP & NP **26**(7), 735–741 (2002). **(in Chinese)**
5. S.N. Fu, Study on the field tuning method of a resonantly coupled RFQ. HEP & NP **26**(8), 870–875 (2002). **(in Chinese)**

6. H.F. Ouyang, S.N. Fu, Tuning and measuring of RFQ with resonantly coupled segments. HEP & NP **27**(6), 551–554 (2003). **(in Chinese)**
7. H.F. Ouyang, S.N. Fu, X.L. Guan et al., Study on the design of an intense-beam RFQ with stabilization. HEP & NP **28**(7), 753–757 (2004). **(in Chinese)**
8. H.F. Ouyang, T.G. Xu, X.L. Guan et al., Computer simulation study on the design of the coupling cell in an RFQ with intense beams. High Power Laser Part. Beams **15**(2), 195–198 (2003). **(in Chinese)**
9. S.N. Fu, H.F. Ouyang, T.G. Xu, Study on the function of dipole stabilizer rods in an RFQ accelerator. HEP & NP **29**(3), 295–300 (2005)
10. L.M. Young, Segmented resonantly coupled Radio-Frequency Quadrupole (RFQ), in *Proceedings of PAC*, *Washington DC*, *USA* (1993), pp. 3136–3138. https://doi.org/10.1109/pac.1993.309578
11. L.M. Young, D.E. Rees, L.J. Rybarcyk et al., High power RF conditioning of the LEDA RFQ, in *Proceedings of PAC*, *New York*, *USA* (1999), pp. 881–883. https://doi.org/10.1109/pac.1999.795387
12. E. Fagotti, L. Antoniazzi, A. Palmieri et al., High-power RF conditioning of the TRASCO RFQ, in *Proceedings of LINAC, Tel-Aviv, Israel* (2012), pp. 828–830
13. H. Shi, H.F. Ouyang, G. Wu et al., Cold measurement and CW conditioning of RFQ for China-ADS Injector-I, in *Proceeding of The Eighth proseminar of Chinese Microwave and Radio Frequency Technology for Accelerator*, *Chendu*, *China* (2016), pp. 6–11 **(in Chinese)**
14. Computer Simulation Technology (CST). https://www.cst.com
15. C.G. Yao, *Electron Linear Accelerator* (Scientific Press, Beijing, 1986). **(in Chinese)**
16. High Frequency Structure Simulator (HFSS). http://www.ansys.com/products/electronics/ansys-hfss
17. H. Shi, H.F. Ouyang, High-power RF conditioning of China ADS 325 MHz RFQ, in *HPPA Mini-Workshop*, *Lanzhou*, *China* (2015)
18. T.M. Huang, Q. Ma, W.M. Pan et al., High power input couplers for China ADS project, in *HPPA Mini-Workshop*, *Lanzhou*, *China* (2015)
19. ANSYS. http://www.ansys.com/
20. C. Meng, S.C. Wang, J.S. Cao et al., Beam commission of C-ADS injector-I RFQ accelerator, in *Proceedings of IPAC*, *Richmond*, *VA*, *USA* (2015), pp. 3827–3829
21. F. Yan, Front end commissioning for China-ADS Injector-I test facility, in *ICFA Mini-Workshop on Beam Commissioning for High Intensity Accelerators*, *Dongguan*, *Guangdong*, *China* (2015)
22. F. Yan, H.P. Geng, C. Meng et al., Commissioning and operation experience with the China ADS Injector-I CW linac. arXiv:1705.05068v1 (2017)